Climate Dynamics
https://doi.org/10.1007/s00382-024-07396-8

ORIGINAL ARTICLE

Oceanic cloud trends during the satellite era and their radiative signatures

George Tselioudis[1] · William B. Rossow[2] · Frida Bender[3] · Lazaros Oreopoulos[4] · Jasmine Remillard[1]

Received: 20 February 2024 / Accepted: 7 August 2024

Abstract
The present study analyzes zonal mean cloud and radiation trends over the global oceans for the past 35 years from a suite of satellite datasets covering two periods. In the longer period (1984–2018) cloud properties come from the ISCCP-H, CLARA-A3, and PATMOS-x datasets and radiative properties from the ISCCP-FH dataset, while for the shorter period (2000–2018) cloud data from MODIS and CloudSat/CALIPSO and radiative fluxes from CERES-EBAF are added. Zonal mean total cloud cover (TCC) trend plots show an expansion of the subtropical dry zone, a poleward displacement of the midlatitude storm zone and a narrowing of the tropical intertropical convergence zone (ITCZ) region over the 1984–2018 period. This expansion of the 'low cloud cover curtain' and the contraction of the ITCZ rearrange the boundaries and extents of all major climate zones, producing a more poleward and narrower midlatitude storm zone and a wider subtropical zone. Zonal mean oceanic cloud cover trends are examined for three latitude zones, two poleward of 50 ° and one bounded within 50°S and 50°N, and show upward or near-zero cloud cover trends in the high latitude zones and consistent downward trends in the low latitude zone. The latter dominate in the global average resulting in TCC decreases that range from 0.72% per decade to 0.17% per decade depending on dataset and period. These contrasting cloud cover changes between the high and low latitude zones produce contrasting low latitude cloud radiative warming and high latitude cloud radiative cooling effects, present in both the ISCCP-FH and CERES-EBAF datasets. The global ocean mean trend of the short wave cloud radiative effect (SWCRE) depends on the balance between these contrasting trends, which in the CERES dataset materializes as a SW cloud radiative warming trend of 0.12 W/m^2/decade coming from the dominance of the low-latitude positive SWCRE trends while in the ISCCP-FH dataset it manifests as a 0.3 W/m^2/decade SW cloud radiative cooling trend coming from the dominance of the high latitude negative SWCRE trends. The CERES cloud radiative warming trend doubles in magnitude to 0.24 W/m^2/decade when the period is extended from 2016 to 2022, implying a strong cloud radiative heating in the past 6 years coming from the low latitude zone.

Keywords Clouds · Radiation · Climate change · Cloud feedbacks

1 Introduction

Clouds modulate both the SW and LW components of the Earth's energy budget and thus play a crucial role in determining the earth's energy imbalance (EEI) which is the primary driver of the ongoing planetary warming (e.g. Loeb et al. 2021; Hansen et al. 2023). Recent studies have shown a near doubling of EEI from 2005 to 2019 in both satellite and in-situ estimates (Loeb et al. 2021). It is therefore crucial to examine and understand cloud property trends in the past decades, in order to better quantify the contribution of cloud property changes to the EEI trends. Cloud properties during the satellite era are derived from operational weather satellite passive radiative retrievals starting in the early 1980s (e.g. ISCCP, CLARA, PATMOS-x), and from research-oriented cloud instrument passive and active retrievals starting in the early 2000s (e.g. MODIS, CloudSat, CALIPSO). This means that a nearly forty-year long record of cloud properties that encompasses several modes of the Earth's shorter

✉ George Tselioudis
george.tselioudis@nasa.gov

1 NASA Goddard Institute for Space Studies, 2880 Broadway, NewYork, NY 10026, USA

2 Franklin, NY, USA

3 University of Stockholm, Stockholm, Sweden

4 NASA Goddard Space Flight Center, Greenbelt, MD, USA

Published online: 18 August 2024

term natural variability (ENSO, PDO) is currently available, and it provides a first estimate of longer-term climate trends. While existing cloud products have different sources of uncertainty and different limitations (Stubenrauch et al. 2013, 2024), using them in conjunction can compensate for several of their limitations and provide more reliable estimates of cloud property trends.

Cloud property temporal trends have been previously studied with the available satellite record of the time. Bender et al. (2012) examined changes in International Satellite Cloud Climatology Project (ISCCP D-version, Rossow and Schiffer 1999) cloud cover in the global midlatitude zones and found a significant poleward shift as well as a narrowing of the extratropical storm track cloudiness. A global analysis of ISCCP and Pathfinder Atmosphere Extended (PATMOS-x, Heidinger et al. 2013) cloud properties by Norris et al. (2016) found cloud change patterns consistent with a poleward retreat of the extratropical storm tracks and an expansion of the subtropical dry zones. Tropical cloud and precipitation trend analyses have found a zonal contraction and a strengthening of the intertropical convergence zone (ITCZ) in the recent decades (Wodzicki and Rapp 2016; Byrne et al. 2018). A similar ITCZ contraction and strengthening was simulated in climate warming model simulations (Lau and Kim 2015). Furthermore, the cloud regime analysis of Tan et al. (2015) found for the same period increases in organized deep convection in the core of the ITCZ region with decreases in less organized convection at the edges of that region.

In parallel with the cloud trend analyses, observational studies have looked at the changes in the position and strength of the primary dynamical features of the Earth's general circulation in the past decades and their relationships with cloud changes. Several studies have found evidence of a tropical expansion and a poleward extension of the Hadley cell (e.g. Grise et al. 2018; Staten and Coauthors, , 2020). Some earlier studies detected only weak signals of poleward midlatitude jet shifts (Archer and Caldeira 2008), but the more recent and time-extensive study of Woollings et al. (2023) found more notable poleward shifts of the midlatitude jets that are consistent across seasons and hemispheres. Tselioudis et al. (2016) examined the relationship between shifts in both Hadley cell extent and midlatitude jet location, and the position of major ISCCP cloud types and found strong correlations only between midlatitude high cloud poleward shifts and Hadley Cell poleward extension. Bender et al. (2012) concluded that the poleward shift in midlatitude cloudiness is supported by a shift in the central position of the mid-troposphere meridional temperature gradient.

The present study extends in time and expands in space the 25 year (1984–2008) ISCCP-D midlatitude cloud trend analysis of Bender et al. (2012), by examining cloud property trends in the 35 year ISCCP-H period (1984–2018) for the global ocean regions. For this 35-year period the study analyzes cloud trends from the ISCCP, PATMOS-x, and CLARA-A3 (Karlsson et al. 2023) satellite datasets and uses the ISCCP-FH satellite radiative flux datasets to investigate associated changes of cloud radiative effects. As these data products are based on operational weather satellites and include a number of record inhomogeneities (see next section) especially in the first decade, we also compare with the more recent 19 year period 2000–2018, when the ISCCP-H dataset is derived from a near fixed number of satellites thus eliminating changes of satellite view zenith angle, and when cloud property data from MODIS and CloudSt/CALIPSO retrievals and radiative flux data from CERES observations are available. With the trend analysis repeated for this more recent period, comparisons between the different datasets and periods can be performed to better account for uncertainties and limitations associated with the different satellite platforms.

2 Datasets and methods

Analysis of global cloud property variations over the entire satellite era, from about 1980 onward, is only possible with cloud datasets derived from operational weather satellites. The first such cloud product was produced by the international satellite cloud climatology project (ISCCP) of the World Climate Research Program (Schiffer and Rossow 1983). The third version of this product is ISCCP-H (Young et al. 2018; Rossow et al. 2022) and currently covers the period 1983–2018. The ISCCP dataset uses both polar orbiting and geostationary satellites to resolve diurnal cloud variations at 3-h intervals with global coverage. A major challenge is to cross-calibrate different imaging instruments (Rossow et al. 2022). The anchor of the whole record is a calibrated radiance dataset from the series of "afternoon" polar orbiters: the residual trend in the Visible calibration is 1.3% increase per decade at a reflectance of about 80%, accompanied by a very small decrease of 0.4% per decade at a reflectance of about 5% (Rossow and Ferrier 2015). Calibration changes affect cloud type identifications, but do not affect retrieved total cloud amounts (Appendix 2 in Stubenrauch et al. 2012). In the first 15 years of the record, failures and relocations of some satellites and the lack of geostationary data over the Indian sector introduced regional changes of cloud properties that contributed to an approximate 30% overestimate of the cloud cover trend in that first period (Rossow et al. 2022), but these effects are not present after July 1998. Attempts to "empirically correct" the ISCCP total cloud amount for the changes of satellite viewing angle (e.g. Norris and Evan 2015; Norris et al. 2016; Knapp et al. 2021) tend to remove the thinnest cloud types and therefore their contribution the cloud amount trend.

The ISCCP cloud products have been used, together with other datasets characterizing the surface and cloudless atmosphere, to calculate radiative flux profiles and the effects of clouds on them (ISCCP-FH, Zhang and Rossow 2023), and this dataset is used here to examine cloud radiative trends for the entire satellite era.

Three other long-term cloud products are based on the AVHRR instrument aboard polar orbiting satellites; the latest versions of the two that use all available satellites are considered here, CLARA-A3 (Karlsson et al. 2017, 2023) and PATMOS-x (Heidinger et al. 2013). Cross-calibration of the different instruments (used by both analyses) is a source of uncertainty of similar magnitude as for ISCCP (Heidinger et al. 2010; Rossow and Ferrier 2015). Although these polar orbiting products provide diurnal sampling at roughly 6 h intervals, inconsistencies over the long record have resulted from the gradual drifting of equatorial crossing times, especially for the "afternoon" series, and from variations in the number of satellites included. These produce uncertainty in long-term variations for certain cloud types and regions that have pronounced diurnal cycles. As will be noted later, the results for CLARA and PATMOS-x cloud trends are very similar, so detailed results will only be presented for CLARA-A3 when comparing with ISCCP for the common period 1983–2018.

Starting in 2000 with the launch of the polar orbiting Terra satellite (and Aqua in 2002), the MODIS instruments provide cloud property data products (Platnick et al. 2021), while the CERES instruments measure top-of-atmosphere radiative fluxes (Loeb et al 2018). Because the orbits of these satellites were fixed until recently, there are no effects of changing view angle or time-of-day sampling. Moreover, calibration of the two MODIS instruments is much better monitored (Xiong and Butler 2020). In 2006, CloudSat (Stephens et al. 2002), carrying the CPR cloud radar, and CALIPSO (Winker et al. 2009), carrying the CALIOP lidar, were launched. Although their spatial sampling is more limited, they provide a completely different sensitivity to clouds that can be used to interpret the results of the imaging instruments.

All these cloud products and several more have been compared in detail in an updated GEWEX Cloud Assessment (Stubenrauch et al. 2024), and the differences and sources of discrepancies between them are now better understood. In the analysis that follows, the latitudinal trends of basic cloud and radiation properties from these datasets are examined for their respective periods of availability. As mentioned before, empirical adjustments to the ISCCP and PATMOS-x datasets have been introduced in the past (e.g. Norris and Evan 2015; Knapp et al. 2021) that attempt to correct biases related to satellite drift, zenith angle, and calibration issues. Those adjusted datasets tend to remove both global mean cloud trends and optically thin clouds along with their trend contributions. In this study, such adjusted or empirically corrected datasets are not considered, but uncertainties in the longer-term dataset trends are rather evaluated through comparisons for the post-2000 period with the MODIS trends which are largely unaffected by zenith angle and calibration issues.

3 Results

3.1 a) Zonal total cloud cover trends in the 1984–2018 period

Hovmöller plots of the time evolution of the zonal, annual mean total cloud cover (TCC) similar to those in Bender et al. 2012 but for the global ocean domain, are examined first. Figure 1 shows the zonal, annual mean Total Cloud Cover Hovmöller diagrams from ISCCP-H data for the period 1983–2018, for the Atlantic and the Pacific Ocean basins. The lines on the plot represent the linear fit to the 80% TCC isoline, chosen to approximate the borders of the two high-TCC midlatitude zones, and the linear fit to the 65% TCC isoline, chosen to approximate the borders of the two low-TCC subtropical zones. Solid lines indicate statistically significant linear trends. The main feature on the plot is the expansion, primarily poleward and to a lesser degree equatorward, of the low-TCC subtropical zones in both hemispheres, which results in a pronounced increase of the extent of those zones in both ocean basins over the 35 year period. On their poleward side the subtropical zone expansion coincides with a poleward shift in all basins of the high-TCC midlatitude storm zone, consistent with the results of Bender et al. (2012) for the shorter 1982–2008 period. In the Southern midlatitude storm zone, the poleward high-TCC shift occurs on both sides but is somewhat stronger on the equatorward side, resulting in only a small midlatitude storm zone narrowing, while in the Northern midlatitudes the poleward shift occurs only on the equatorward side resulting in a more significant narrowing of the storm zones. On the equatorward side of the two low-TCC subtropical zones, the simultaneous expansion of the Northern and Southern zones results in a significant contraction of the inter tropical convergence zone (ITCZ), which is more pronounced in the Atlantic Ocean basin. Note that the near merging of the 65% isolines of the Atlantic ITCZ in the later years does not signify a disappearance of the climate zone but rather a simultaneous reduction of the zone's extent and its TCC (by about 10%). In the Pacific Ocean the ITCZ contraction is smaller and the TCC decrease is around 5%. This ITCZ contraction mirrors the findings of Wodzicki and Rapp (2016) for the Pacific Ocean based on precipitation trends seen in the tropical rainfall measuring mission

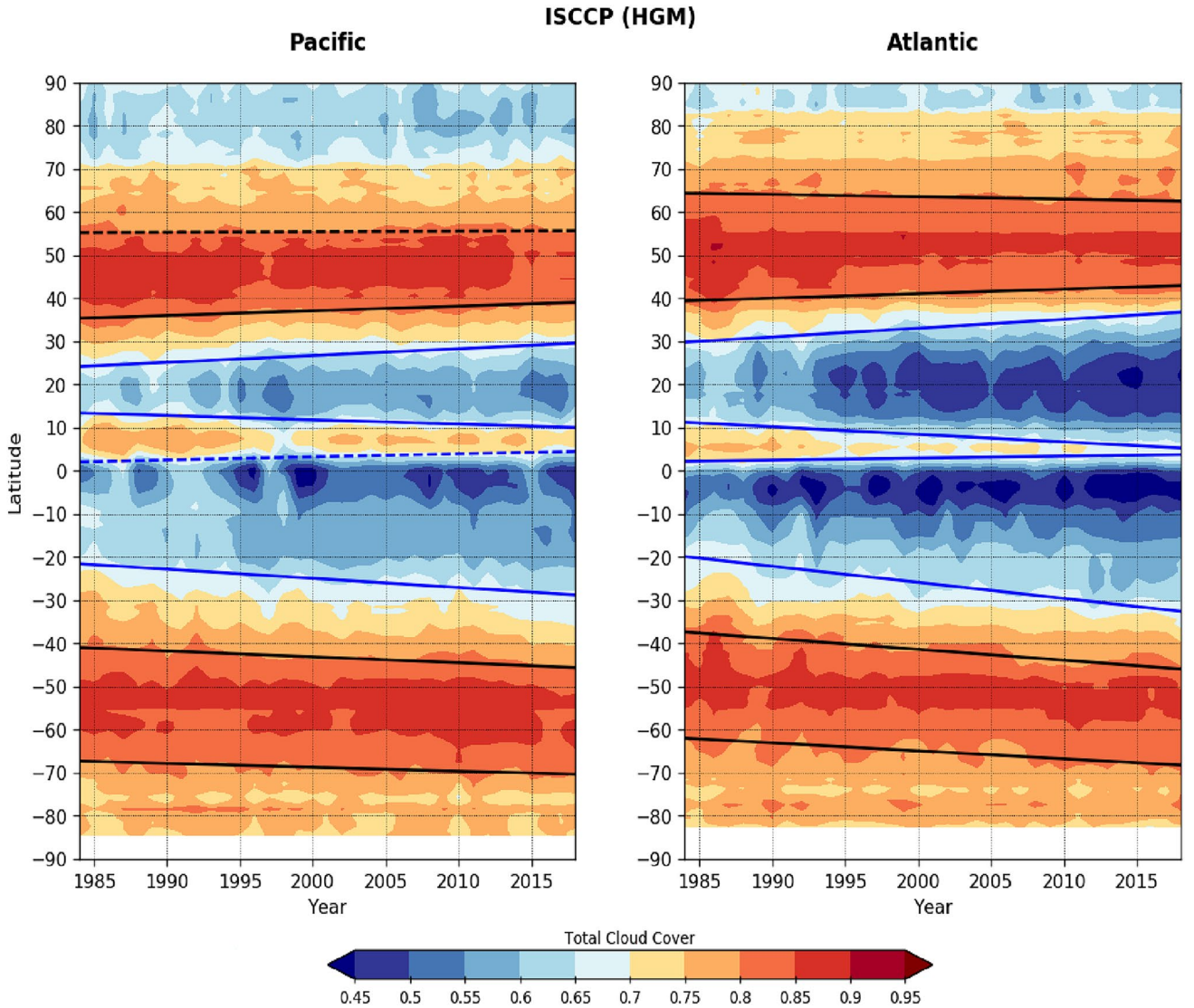

Fig. 1 Hovmöller plots of ISCCP-H zonal, annual mean TCC for 1984–2018, for the Pacific (left) and the Atlantic (right). Blue lines show the 65% and black lines the 85% TCC isolines. Solid lines indicate statistically significant trends at the 95% significance level

(TRMM) and the global precipitation climatology project (GPCP) datasets.

Figure 2 uses the same line definitions and color bar as Fig. 1 to show the zonal, annual mean TCC Hovmöller diagram for the CLARA-A3 dataset. The expansion of the subtropical low-TCC zone is similarly pronounced in the CLARA-A3 dataset, as is the resulting contraction of the ITCZ zone, but both show somewhat smaller magnitudes than in the ISCCP plot. The midlatitude high-TCC zones also shift poleward in both hemispheres and oceans in a similar manner to ISCCP, but the poleward part of the Southern midlatitude zone shifts equatorward in both oceans significantly contracting the zones, something not seen in ISCCP. Note that all three satellite product descriptions specifically indicate reduced accuracy in cloud detection in the polar regions (Heidinger et al. 2014; Karlsson et al. 2017; Rossow et al. 2022) and therefore the TCC trends are less reliable poleward of about 70 degrees in both Hemispheres. A Hovmöller plot of annual, zonal mean TCC for the PATMOS-x dataset (Fig. S1) shows features that are very similar to those found in the CLARA-A3 dataset.

A quantitative depiction of the cloud zone shifts in the ISCCP and CLARA-A3 datasets shown in Figs. 1 and 2 is presented in Table 1, which provides the slopes of the linear fits to the 80% and 65% TCC isolines in the two basins and datasets. Note that positive values indicate northward shifts while negative values indicate southward shifts, and bold numbers denote statistically significant shifts. The values show that the two datasets agree with the two-sided expansion of the subtropical zones, but ISCCP gives values that

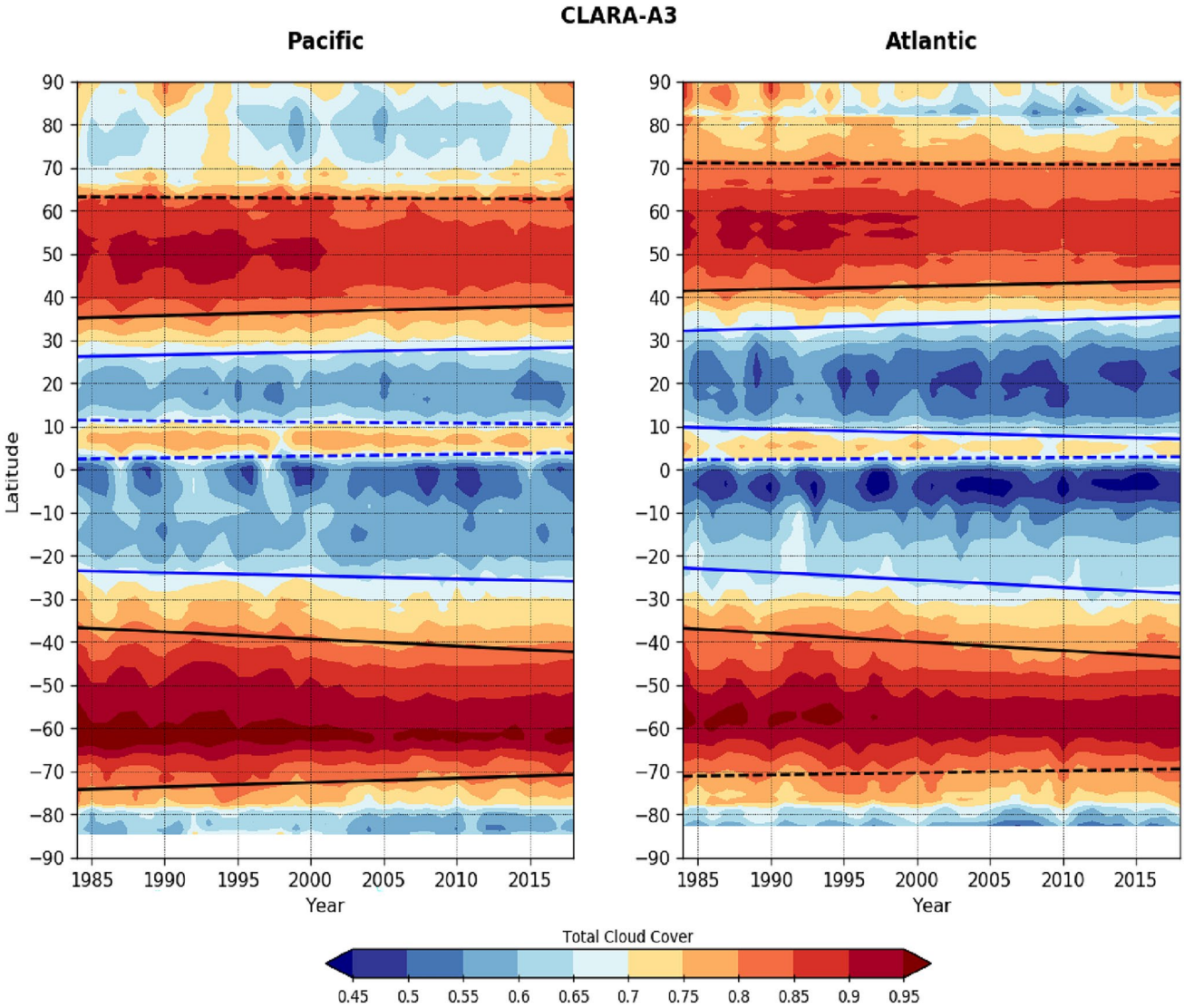

Fig. 2 As in Fig. 1 for the CLARA-A3 dataset

Table 1 TCC Isoline Trends (*1984-2018 in deg/decade*)

	Pacific		Atlantic	
	ISCCP	CLARA	ISCCP	CLARA
80% NH High Latitudes	0.12	-0.16	**-0.55**	-0.11
80% NH Midlatitudes	**1.09**	**0.87**	**1.05**	**0.67**
65% NH Subtropics	**1.59**	**0.64**	**2.04**	**0.99**
65% NH Tropics	**-1.00**	-0.27	**-1.76**	**-0.80**
65% SH Tropics	0.71	0.40	**0.45**	0.20
65% SH Subtropics	**-2.13**	**-0.71**	**-3.74**	**-1.75**
80% SH Midlatitudes	**-1.36**	**-1.66**	**-2.52**	**-2.00**
80% SH High Latitudes	**-0.89**	**1.01**	**-1.85**	0.51

*Slopes of linear fits to the 80% (red) and 60% (blue) TCC isolines for ISCCP and CLARA-A3 and the Pacific and Atlantic Oceans, as depicted in Figs. 1 and 2. Positive/negative slopes indicate Northward/Southward direction, and bold numbers indicate linear fits significant at the 95% level.

range from 1.59–3.74 degrees per decade for the poleward expansion and 0.45–1.76 degrees per decade for the equatorward one, while CLARA-A3 gives values of 0.64–1.75 degrees per decade for the poleward and 0.27–0.80 degrees per decade for the equatorward expansion. They also broadly agree in the magnitude (~ 1–2.5 degrees per decade) of the poleward shift of the equatorward side of the midlatitude zones but disagree in the sign of the shift of the poleward sides of the midlatitude zones.

The values in Table 1 can be used to provide another perspective on the tropical expansion that has been observed in several observational studies over the past few decades (e.g. Seidel et al. 2008, Staten and Coauthors 2020). These studies used primarily dynamical and hydrologic indices to determine the poleward edge of the Hadley cells and defined the width of the tropics as the zone between the Northern and

Southern Hemisphere Hadley cell edges. The present study uses the 65% TCC isoline to define the edges of the low-TCC subtropical zone and therefore can provide a measure of both the width of the global tropics, defined as the region between the poleward edges of the two low-TCC zones, but also the width of the ITCZ, defined as the region between the equatorward edges of the two low-TCC zones. For the width of the tropics, the values in Table 1 show a tropical expansion for ISCCP of 3.72 deg/decade in the Pacific and 5.78 deg/decade in the Atlantic, and for CLARA a tropical expansion of 1.35 deg/decade in the Pacific and 2.74 deg/decade in the Atlantic. These values fall on the high end or, in the case of ISCCP, are higher than the 0.25–3 deg/decade range found in the dynamical studies (Staten et al. 2020). Note however that the present study examines only the two ocean basins rather than the global domain. For the contraction of the ITCZ, ISCCP shows values of 1.71 deg/decade in the Pacific and 2.21 deg/decade in the Atlantic while CLARA shows values of 0.67 deg/decade in the Pacific and 1 deg/decade in the Atlantic. For the Pacific ITCZ, the analysis of Wodzicki and Rapp (2016) finds a contraction of about 0.6 deg/decade for the 1980–2014 period.

The expansion of the subtropical zones alters the zonal cloud distribution by expanding the domain of the low-TCC regimes. However, Figs. 1 and 2 show that cloud cover trends also vary within each climate zone, so the latitude-resolved trends are examined next. Figure 3 shows the zonal, annual mean trend in TCC for the combined Atlantic and Pacific oceans over the 35-yr period (1984–2018) for ISCCP and CLARA-A3. In ISCCP, two regions of contrasting cloud cover trends emerge from the analysis. A low latitude region, between 50S and 50N, where TCC shows significant decreasing trends, and a high latitude region, poleward of 50N/S where TCC either increases in the southern region or shows near-zero trends in the northern one. In the low latitude region, the poleward expansion of the subtropical zone creates the TCC decreases in the 25°–40°N/S zone, a feature also found in the analysis of an empirically corrected version of the ISCCP-D dataset (Norris et al. 2016) for a shorter time period (1983–2009). A relatively weaker TCC decreasing trend coincides with the ITCZ, but stronger decreases are found to the north and south caused by both the equatorward expansion of the subtropical zones and by zonal TCC decreases near 5°S and 20°N. In the southern high latitude region TCC increasing trends are found, caused in part by the poleward expansion of the midlatitude zone, while in the northern high latitude region the lack of such expansion makes TCC trends negligible. Note however that polar regions suffer from large TCC satellite retrieval uncertainties and that there is low ocean coverage poleward of 70 degrees. Differences in Table 1 between ISCCP and CLARA in the magnitude and sometimes the sign of some TCC isoline trends also result in somewhat different latitudinal variations

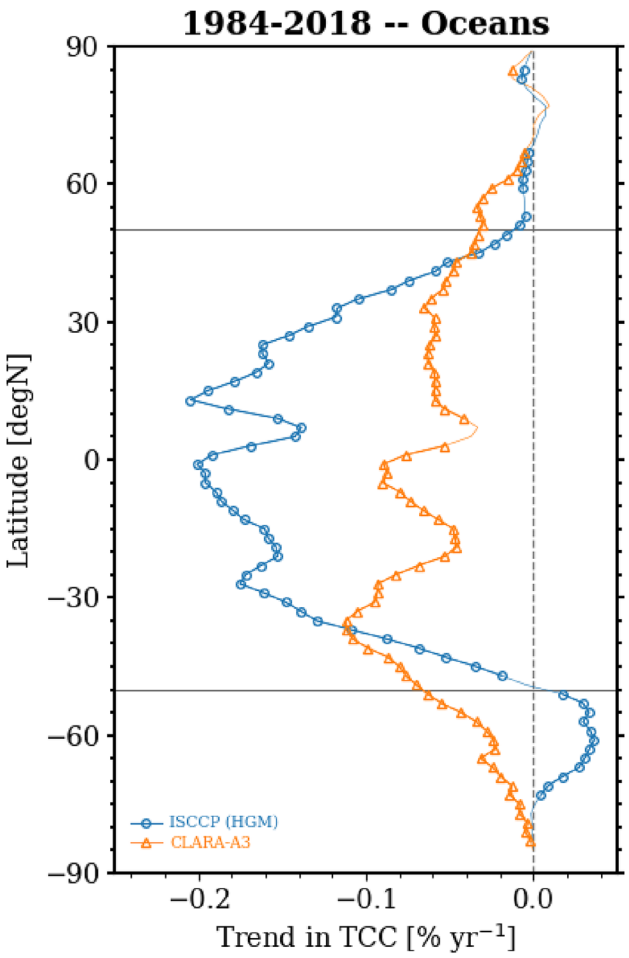

Fig. 3 Zonal, annual mean TCC trends for the 1984–2018 period, for the ISCCP-H and CLARA-A3 datasets. The data are plotted for 2-degree wide latitude zones weighted by the cosine of latitude and the ocean fraction. Symbols and thick lines indicate latitude zones with significant trends at the 95% significance level

in zonal cloud cover trend between the two datasets. In the low latitude zone, both datasets show decreasing TCC trends with ISCCP showing trend values on average almost double on average than those of CLARA-A3. In the Northern high latitude zone both datasets show near-zero TCC trends, but in the Southern high latitude zone their trends have opposite signs, upward for ISCCP, and downward for CLARA-A3.

3.2 b) Zonal total cloud cover trends in the 2000–2018 period

For the period 2000–2018 when the ISCCP-H dataset is derived from a constant number of satellites, a cloud property dataset from the MODIS instrument retrievals (Platnick et al. 2021) is also available, specifically from Collection 6.1. Therefore, for that period all of the MODIS, ISCCP-H, and CLARA-A3 datasets can be examined in conjunction

with regard to their zonal TCC trends. Hovmöller diagrams of the time evolution of the zonal, annual mean TCC were derived first, and the plots (not shown here) revealed the same subtropical zone expansion and ITCZ narrowing in all three datasets, but with less significant linear trends due to the shorter length of the time series. The slopes of the different isolines for ISCCP, CLARA-A3, and MODIS are shown in Table S1. The sign of the trends remains the same as in the longer 35-year period, with the subtropical low-TCC zones expanding on both sides, the ITCZ contracting, and the midlatitude zones shifting poleward, but as expected the significance and magnitude of the trends is much lower compared to the longer period. The ISCCP analysis shows a tropical expansion of 2.07 deg/decade in the Pacific and 2.77 deg/decade in the Atlantic, CLARA-A3 shows an expansion of 1.03 deg/decade in the Pacific and 1.00 deg/decade in the Atlantic, while MODIS shows an expansion of 1.07 deg/decade in the Pacific and only 0.17 deg/decade in the Atlantic. For the ITCZ contraction, ISCCP gives values of 0.67 deg/decade for the Pacific and 1.16 deg/decade for the Pacific, CLARA-A3 gives values of 0.95 deg/decade in the Pacific 0.61 deg/decade in the Atlantic, while MODIS gives values of 1.30 deg/decade in the Pacific and 0.17 deg/decade in the Atlantic.

The zonal, annual mean TCC trends for ISCCP, CLARA, and MODIS for the 2000–2018 period are shown in Fig. 4. The MODIS-derived TCC trends are very similar between the Terra and Aqua instruments, so we show here only the trends from MODIS-Terra since they allow for a longer comparison period. The dominant feature is that all three datasets exhibit a consistent pattern between the three zones, with upward or near-zero TCC trends in the high latitude zones and downward TCC trends in the low latitude zone. The ISCCP trend pattern for this 19-year period is similar to the longer 35 year period, with strong TCC decreases in the low latitude zone, increases in the Southern high latitudes and imperceptible changes in the Northern high latitudes. For this shorter period CLARA-A3 shows almost no trend in the Southern high latitudes and upward trends in the Northern high latitudes along with the consistent downward trends in the low latitude zone. The MODIS analysis shows upward TCC trends in both high latitude zones, and downward TCC trends in the low latitude zone that are somewhat stronger than CLARA-A3 in the Southern Hemisphere but significantly weaker than ISCCP at most low latitudes.

In addition to the passive retrievals of cloud properties analyzed so far, active retrievals from radar (CloudSat) and Lidar (CALIPSO) measurements are available for shorter parts of the 2000–2018 time period and can be added as an independent cloud cover measurement to the cloud cover trend comparisons. Figure 5 shows the zonal, annual mean TCC trends from ISCCP, CLARA-A3, and MODIS together with those derived from the combined CloudSat/CALIPSO

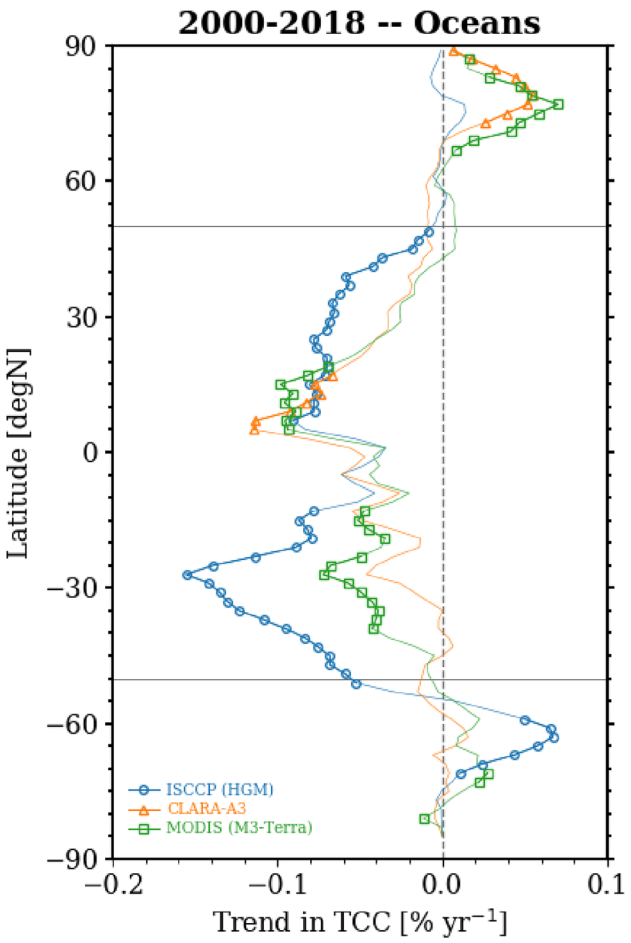

Fig. 4 Zonal, annual mean TCC trends for the 2000–2018 period, for the ISCCP-H,CLARA-A3, and MODIS datasets. The data are plotted for 2-degree wide latitude zones weighted by the cosine of latitude and the ocean fraction. Symbols and thick lines indicate latitude zones with significant trends at the 95% significance level

3S-GEOPROF-COMB dataset (Bertrand et al. 2023) for their common time period 2007–2016. The plot shows that ISCCP, MODIS, and 3S-GEOPROF-COMB trends agree well in their overall structure, with weak TCC increases in the high latitude zones and strong decreases in the low latitude zone outside the equator, while CLARA-A3 shows similar increases in the high latitude zones but weaker decreases and even some increasing trends in the low latitude zone. The close correspondence between the passive (especially ISCCP and MODIS) and active (radar and lidar) TCC trend zonal patterns for this shorter period strengthens our confidence in the robustness of the trends derived from those instruments for the longer time periods.

Figure 6 provides a summary of the oceanic TCC annual trends for the three climatic zones and the global ocean, derived from the different datasets for their respective periods. For the low latitude zone, agreement is found in all datasets and periods that a significant and consistent (as

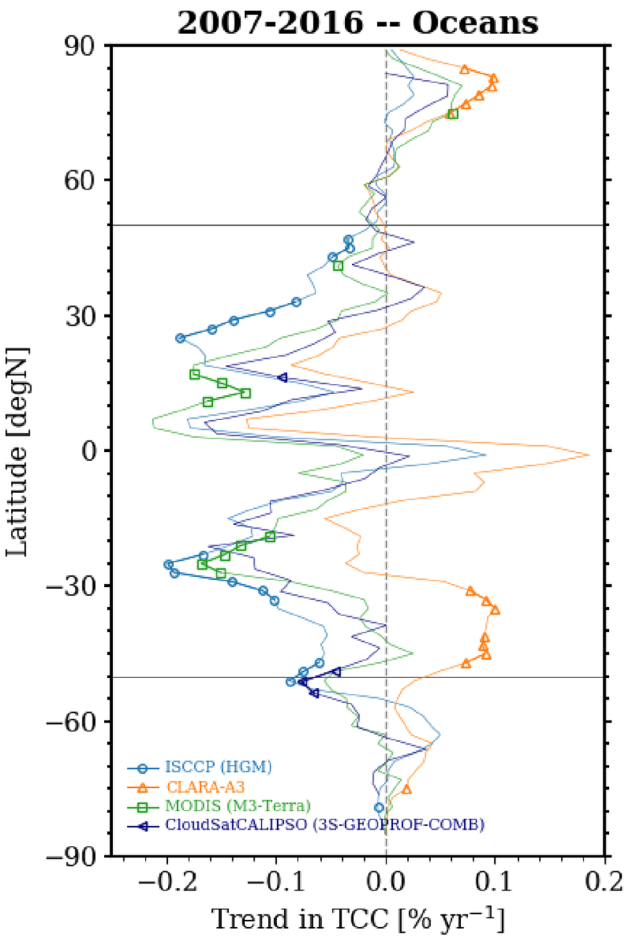

Fig. 5 Zonal, annual mean TCC trends for the 2007–2016 period, for the ISCCP-H, CLARA-A3, MODIS, and CloudSat/CALIPSO datasets. The data are plotted for 2-degree wide latitude zones weighted by the cosine of latitude and the ocean fraction. Symbols and thick lines indicate latitude zones with significant trends at the 95% significance level

indicated by the uncertainty bars) downward TCC trend is observed. The trend in ISCCP is nearly double that of CLARA-A3 and MODIS, and for both ISCCP and CLARA-A3 the trend is almost half as strong in the 19 year as in the 35 year record implying a weakening of the trend with time. In the Southern high latitudes, ISCCP shows a consistent upward TCC trend in both periods and MODIS shows also an upward trend of somewhat smaller magnitude for the shorter 19 year period. CLARA-A3 on the other hand shows a downward TCC trend in the longer period and a near-zero trend in the shorter period. In the Northern high latitudes, ISCCP shows near-zero trends in all periods while CLARA-A3 changes from a downward to an upward trend in the later period and MODIS shows a consistent upward trend in that period. The global ocean TCC trend is dominated by the more extensive low latitude zone and is negative for all datasets and periods. This global downward trend for the 35-year period is 0.72% per decade for ISCCP and 0.45% per decade for CLARA-A3, while for the more recent 19 year period it is weaker and ranges from 0.17% per decade for MODIS and CLARA-A3 to 0.39% per decade for ISCCP. For the negative global ocean trend, despite the mean value differences all three datasets show significant ranges of overlap.

Examining in more detail the differences in TCC trends between the different satellite datasets shown in Fig. 6, it can be said that qualitatively all three datasets show trends of the same sign for all regions and periods except for ISCCP-H and CLARA-A3 for the 35 year period in the Southern high latitudes. Between the two datasets, ISCCP-H has the advantage of better and constant diurnal sampling, which is important for the diurnally varying low clouds at low latitudes, but the disadvantage of lack of geostationary data over the Indian sector in the early part of the record with potential field of view issues at the higher latitudes. While it is hard to assess the ultimate impact of these advantages

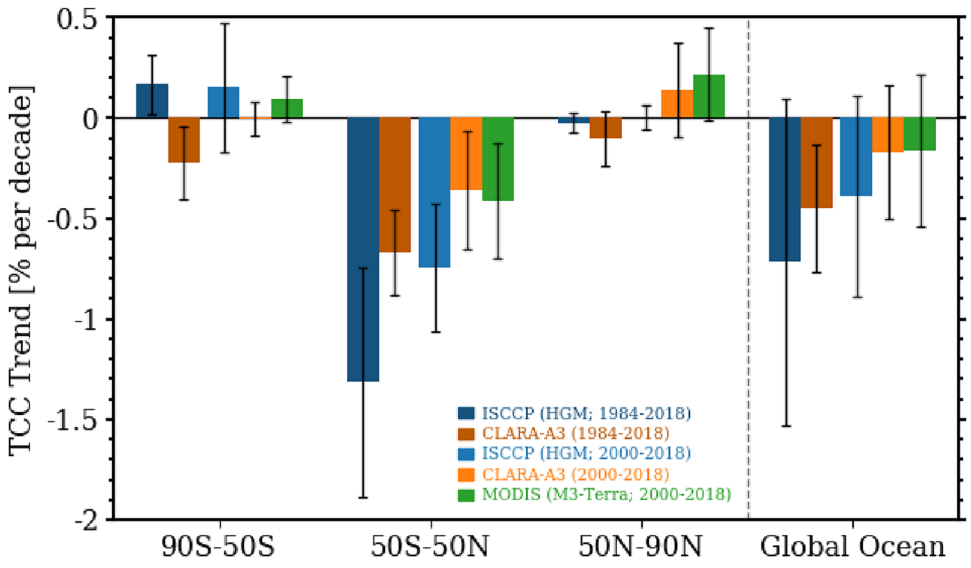

Fig. 6 Bar graph of the annual mean TCC trends in %/decade for the high latitude zones (50N/S-90N/S), the low latitude zone (50S-50N), and the global Oceans, for the ISCCP-H and CLARA-A3 35-year (1984–2018) and 19-year (2000–2018) periods, and for the MODIS 19-year period. The uncertainty bars indicate the 2σ (σ-standard deviation) range of the TCC values within each zone

and disadvantages, it is important to note that for the 19 year period in the same region ISCCP-H shows again a positive trend that is in agreement with MODIS while CLARA-A3 changes from a strong negative to a weak positive trend. Quantitatively, ISCCP-H shows stronger decreasing trends in the low latitudes than both CLARA-A3 and MODIS, but with overlapping uncertainty ranges between the datasets. The very large decreasing trend in ISCCP-H for the 35 year period may be affected by the Indian ocean data issues, but CLARA-A3 also shows a stronger trend in the longer than in the shorter period. Overall, it is important that trends from MODIS which has poor diurnal coverage at low latitudes but is less subject to calibration uncertainties and can thus be considered as more stable, are qualitatively in agreement with the other two datasets for the same periods and regions.

3.3 c) Zonal cloud radiative effect trends in the satellite era

Two radiative flux datasets are used here to examine the trends in shortwave cloud radiative effect (SWCRE) during the satellite era. One is the ISCCP-FH dataset, which is a radiative flux dataset derived using as input the cloud and atmospheric property retrievals of the ISCCP-H dataset (Zhang and Rossow 2023). It covers the 1983–2017 period, and it provides SWCRE values and trends that are fully consistent with the ISCCP-H underlying cloud properties. The other is the CERES-EBAF dataset, which provides radiative flux measurements from the CERES instrument on Terra and Aqua and covers the period from 2000 to the present (Loeb et al. 2018). The SWCRE values are based on irradiances derived from a radiance to flux conversion enabled by angular distribution models (ADMs), which depend on scene identification provided by MODIS on the same platforms. The SWCRE trends are examined for three different periods: the 35 year period from 1983–2017 when ISCCP-FH is available, the 18 year period from 2000–2017 when both ISCCP-FH and CERES are available, and the 23 year period from 2000–2022 which is the full period covered by the CERES dataset.

The zonal SWCRE trends for the two datasets and the three periods are shown in Fig. 7. Since SWCRE is a negative quantity indicating cooling, positive SWCRE trends imply decreased cloud radiative cooling. Overall, a picture emerges that is consistent with the TCC trends presented in Figs. 3 and 4. In the high latitude zones all datasets and periods show negative or near-zero SWCRE trends implying increasing cloud radiative cooling or no radiative change, consistent with the upward or near-zero TCC trends shown earlier. In the low latitude zone the different datasets and periods show mostly positive SWCRE trends indicating less cloud radiative cooling consistent with the downward TCC trends documented earlier. For

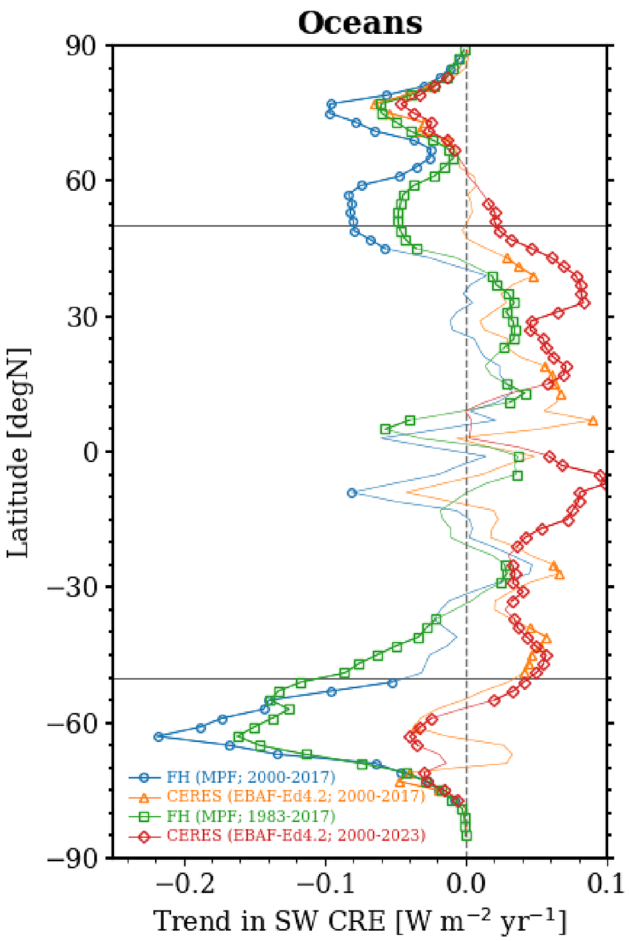

Fig. 7 Zonal, monthly mean SWCRE trends for the ISCCP-FH 1983–2017 and 2000–2017 periods and for the CERES-EBAF 2000–2017 and 2000–2022 periods. The data are plotted for 2-degree wide latitude zones weighted by the cosine of latitude and the ocean fraction, and symbols indicate latitude zones with significant trends at the 95% significance level

ISCCP-FH, at the high latitude zones and the poleward edges of the low latitude zone significant cloud SW cooling is found, while only in the 30°S-30°N region weak to moderate cloud radiative warming is present. This behavior is consistent in both the short and long time periods for ISCCP-FH. The SWCRE tends of ISCCP-FH and CERES are overall qualitatively similar but with notable quantitative differences. In the high latitude zones, the CERES dataset shows mostly negative but much weaker SWCRE trends, while in the low latitude zone it shows more consistent and larger positive SWCRE trends than ISCCP-FH. When the full period for CERES is plotted with the addition of years 2018–2022, the SWCRE positive trend in the low latitude zone becomes noticeably stronger and more significant implying weaker SW cloud radiative cooling in that later period, which is consistent with the recent

increase in the Earth's Energy Imbalance found by Loeb et al. (2021) who attributed it to increased SW absorption.

The low latitude SWCRE warming is weak in the ISCCP-FH dataset (Fig. 7) despite the large TCC downward trend in the same region (Fig. 3 and Fig. 4). The reason is that in the ISCCP-H dataset there is an overall upward trend of cloud optical thickness (TAU) in both the longer and shorter periods, as illustrated in Figure S2. The figure also shows similar trends in optical thickness from MODIS for the shorter time period. The positive TAU trends are larger in the high latitude zones, for both ISCCP-H and MODIS, where they account for a larger SWCRE cooling trend in ISCCP-FH, but are also significant in the low latitude zone where they counteract the radiative effect of the strong TCC decreases thus producing only a weak radiative warming in that region. The ISCCP-H cloud optical thickness trend is overestimated by about a third because of the residual visible calibration trend (Rossow and Ferrier 2015), which produces larger changes for the bigger TAU values than for smaller values consistent with the comparison to MODIS values in Fig. S2. Therefore, the ISCCP-FH SWCRE trend is an overestimate of the high latitude cloud radiative cooling and an underestimate the low latitude cloud radiative warming.

Figure 8 summarizes the SWCRE trends of ISCCP-FH and CERES-EBAF in the three latitude zones, for the ISCCP-FH full 35-year period (1983–2017), for their common 18-year period (2000–2017), and for the CERES-EBAF full 23-year period (2000–2022). In the two high latitude zones, all datasets and periods show SW cloud radiative cooling trends which are larger in ISCCP-FH than in CERES, particularly in the Southern Hemisphere. In the low latitude zone, the CERES dataset shows significant SW cloud radiative warming trends (i.e. weaker cooling) while ISCCP-FH shows very weak radiative cooling trends (i.e. stronger cooling). In the global oceans mean result, the CERES dataset shows a SW cloud radiative warming trend of 0.12 W/m^2/decade coming from the dominance of the more extensive low latitude zone, while the ISCCP-FH dataset shows a SW cloud radiative cooling trend of 0.25–0.35 W/m^2/decade due to the strong cooling trends of the high latitude zones. It is important to note that the full 22 year period of CERES-EBAF shows a doubling of the global SW cloud radiative warming trend (0.24 w/m^2/decade), coming primarily from the doubling of the SWCRE warming in the low latitude zone, a result that further emphasizes the recent increase over the past few years of the absorbed SW radiation and the Earth's Energy Imbalance first demonstrated in Loeb et al. (2021).

The overall picture of SWCRE trends (Fig. 8) show high latitude cloud radiative cooling in all datasets and periods but much stronger in ISCCP-FH than in CERES, and cloud radiative warming in the low latitude zone for CERES but small cooling or zero trends for ISCCP-FH. The CERES SWCRE values are derived from direct flux measurements, with a prior cloud/clear discrimination, while the ISCCP-FH SWCRE values are derived from a radiative flux model with ISCCP-H cloud properties as the primary input. Overall, the CERES SWCRE values are subject to fewer potential uncertainty sources and can be considered more reliable.

4 Summary and discussion

Analysis of the zonal mean total cloud cover (TCC) from three different satellite datasets show an overall expansion of the subtropical low-TCC zone with a concurrent poleward displacement and contraction of the high-TCC midlatitude zone, and a contraction of the tropical ITCZ

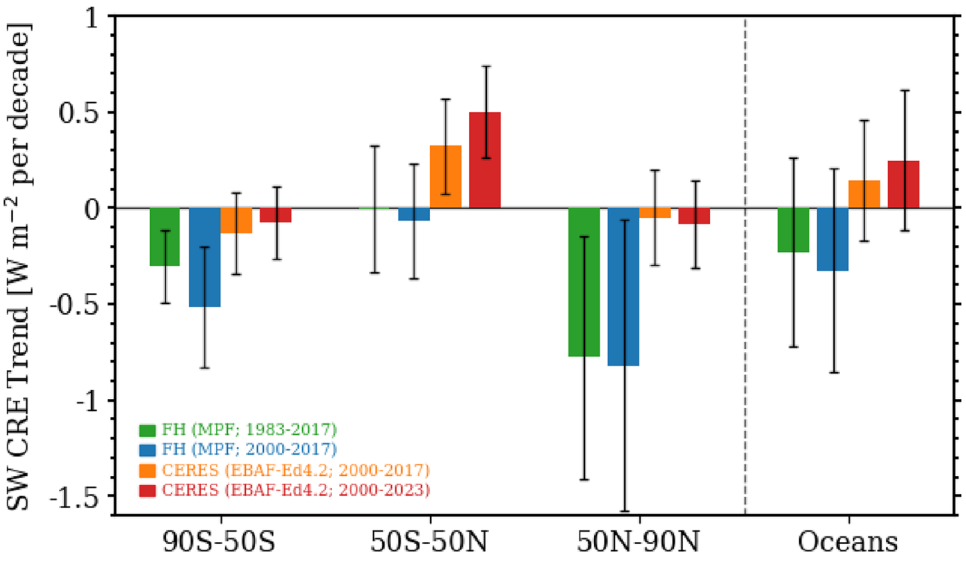

Fig. 8 Bar graph of the monthly mean SWCRE trends in W/m^2/decade for the high latitude zones (50N/S-90N/S), the low latitude zone (50S-50N), and the global Oceans, for the ISCCP-FH 35-year (1983–2017) and 18-year (2000–2017) periods, and for the CERES-EBAF 18-year (2000–2017) and 23-year (2000–2022) periods. The uncertainty bars indicate the 2σ (σ-standard deviation) range of the SWCRE values within each zone

region over the 1984–2018 period. This expansion of the 'low cloud cover curtain' and the contraction of the ITCZ result in a realignment of the boundaries and extents of all major climatic zones. Our study provides a global picture of this oceanic climate zone realignment (Figs. 1 and 2) and derives cloud-based metrics for the expansion of the tropics and the contraction of the ITCZ (Tables 1 and S1). For the expansion of the tropics, the cloud-based metric, when averaged over all periods and ocean basins, gives values that range from 3.5 deg/decade for ISCCP, to 1.5 deg/decade for CLARA-A3, to 0.7 deg/decade for MODIS which only includes the 2000–2018 period and for which period ISCCP and CLARA-A3 also have lower values (2.4 and 1 deg/decade respectively). Previous studies used mostly dynamical indices, such as the mass streamfunction or the surface wind transition, to define the tropical width, and found a wide range of tropical expansion rates depending on methodology and the period examined. An earlier review (Seidel et al. 2008) found a range of 0.25–3 deg/decade, while a more recent review (Staten and Coauthors 2020) found a narrower range of 0.25–0.5 deg/decade, attributing the difference to better metrics and correction of reanalysis spurious trends. The cloud-based metric of tropical expansion presented here shows values at the high end and even higher than the ones derived from the dynamical metrics. This may be due to the fact that clouds respond to a combination of dynamic and thermodynamic cloud controlling factors. For instance, Tselioudis et al. (2016) showed that high-top clouds are the only cloud type that respond in any significant degree to changes in the extent of the Hadley cell or the position of the midlatitude jet. For the narrowing of the ITCZ, the cloud-based metric used in this study gives an average value of about 2.5 deg/decade for ISCCP, 1 deg/decade for CLARA, and 0.7 deg/decade for MODIS which again refers only to the 2000–2018 period. The precipitation-based analysis of Wodzicki and Rapp (2016) found a narrowing of the Pacific ITCZ of 0.6 deg/decade in the 2000–2015 period, which is again at the lower end of the cloud-based numbers. The cloud-based indices of the climate zone realignment show a wide range of values and overall larger trends than the dynamical and precipitation indices, but the universal agreement between all datasets and periods for the sign of those indices provide confidence for a robust tropical expansion and ITCZ and storm cloud contraction during the satellite era.

The global ocean, zonal mean cloud cover trends in all three satellite datasets can be examined in a framework of three latitude zones, a southern and a northern high latitude zone that include ocean areas poleward of 50 °, and a low latitude zone with ocean areas between 50°S and 50°N. In the two high latitude zones, cloud cover trends tend to be either positive or near zero for most datasets and periods, with CLARA showing even negative trends in the 35 year time period. In the low latitude zone, negative TCC trends are present in all periods and datasets, and the negative sign of the trends is consistently inside the 2σ uncertainty range. These strong and consistent low latitude TCC downward trends dominate the global mean picture producing cloud cover decreases that range from 0.72% per decade to 0.17% per decade depending on dataset and period. Such low latitude cloud cover decreases, expressed as decreases in cloud cover with temperature, form the basis of the positive subtropical low cloud feedback documented in Sherwood et al. (2020), Cesana and DelGenio (2021) and other studies. In the present study, the low latitude TCC decreasing trends can be attributed in large part to the expansion of the low-TCC subtropical zones, which reduce cloud cover in the lower midlatitude regions and on the edges of the ITCZ. However, TCC decreases are also found in the core of the low-TCC subtropical zones, which may be related to changes in thermodynamic atmospheric processes rather than shifts in the atmospheric circulation.

These contrasting cloud cover increases and decreases between the high- and low-latitude zones produce, in the CERES-EBAF dataset contrasting low-latitude strong upward SWCRE trends and high-latitude weak downward SWCRE trends, and in the ISCCP-FH dataset low-latitude weak downward or near-zero SWCRE trends and high-latitude strong downward SWCRE trends. The global ocean trend of the SW cloud radiative effect depends on the balance between these contrasting trends, and in the CERES dataset this balance is a SW cloud radiative warming trend of 0.12 W/m^2/decade coming from the dominance of the low-latitude positive SWCRE trends while in the ISCCP-FH dataset it is a 0.3 W/m^2/decade SW cloud radiative cooling trend coming from the dominance of the high latitude negative SWCRE trends. Here it is important to note that the CERES cloud radiative warming trend doubles in magnitude to 0.24 W/m^2/decade when the period is extended from 2016 to 2022, implying a strong cloud radiative heating in the recent years coming from cloud changes in the low latitude zone, in accordance with Loeb et al. (2021). It must also be noted that the strong ISCCP-FH high latitude cloud radiative cooling trend and the muted low latitude cloud radiative warming trend are caused in addition to the TCC changes by a spurious increasing trend in cloud optical thickness, which is in part due to a residual satellite calibration trend.

One question that needs to be explored is what types of clouds are changing with time and producing the observed TCC trends. A previous analysis of trends in ISCCP-H cloud types defined from set cloud optical depth-cloud top pressure (TAU-PC) thresholds, shows that a decrease in the global mean TCC comes primarily from a decrease in the optically thinner cumulus and altocumulus categories (Rossow et al. 2022 but see Fig. 4 in Zhang and Rossow 2023). The GEWEX assessment shows that ISCCP_H has more of these cloud types than the other datasets (Stubenrauch

et al. 2024), which may explain the larger magnitudes of the TCC trends in ISCCP-H. A similar result is obtained in an analysis of Weather States (WSs) derived from the application of a clustering algorithm on ISCCP-D TAU-PC histograms (Tselioudis et al. 2013), which finds decreases in the shallow cumulus WS and corresponding increases in the low-TCC fair weather WS during the 1983–2009 period. However, a more thorough investigation of the zonally resolved TCC trends is necessary, and a study is under way to examine in detail the zonal changes in both the WSs derived from the ISCCP-H dataset (Tselioudis et al. 2021) and in the Cloud Regimes derived from the application of a similar clustering algorithm on TAU-PC histograms derived from MODIS dataset (Oreopoulos et al. 2014; Cho et al. 2021)). Such a regime based analysis can expand from the zonal to the local scales to better explore the effects of processes beyond the mean meridional circulation on the observed cloud trends.

The contrasting TCC trends in the high and low latitude regions indicate the action of a multitude of mechanisms that produce those tends. The expansion of the low-TCC subtropical zone is indicative of a change in the atmospheric general circulation, namely a widening of the Hadley circulation and a shift of the midlatitude storm tracks as found in previous studies (e.g. Grise et al. 2018; Staten et al. 2020; Woollings et al. 2023). Several mechanisms have been proposed that can contribute to the recent tropical widening, including stratospheric ozone depletion, aerosol and ozone forcing, and also coupled atmosphere–ocean variability (Grise and Coauthors 2019). The narrowing and strengthening of the ITCZ found here and in other studies (Wodzicki and Rapp 2016; Byrne et al. 2018) can be another potential forcing of the Hadley cell expansion through additional latent heat release (e.g. Rind and Rossow 1984), and the expansion can be understood in the context of Radiative Convective Equilibrium theory as an offset of the increased tropical latent heating through expanded subtropical radiative cooling (Jakob et al. 2019). The fact that the general atmospheric circulation is enhanced is also suggested by the changes of the meridional longwave cooling associated with the cloud changes in the ISCCP-FH fluxes (Zhang and Rossow 2023). However, TCC trends are also observed within the core of the latitude zones which indicate that local mechanisms rather than large scale shifts are also at play. At high latitudes such mechanisms can be related to transitions from ice to water cloud particles as temperature warms which can result in both larger cloud amounts and larger cloud optical depths through the 'cloud phase feedback' (Mitchell et al. 1989; Tan et al. 2016; Frey & Kay 2017). The low latitude TCC decrease that occurs in all datasets and dominates the global TCC trend (Fig. 6) can be the result of cloud reduction mechanisms related to changes in boundary layer depth, relative humidity in the cloud layer, or convective moistening rate and large-scale humidity advection at the top of the boundary layer (e.g. Webb et al. 2024). In addition, indirect effects from aerosol decreasing trends can be playing a role in the low latitude TCC decreases, as well as in the strengthening of the cloud radiative warming in the past few years shown in Fig. 7. The present study provides a global scale framework that can be used to construct a unified theory of the combined effects of dynamical, thermodynamical, and microphysical processes on global cloud field variability and the resulting cloud and radiation trends.

Supplementary Information The online version contains supplementary material available at https://doi.org/10.1007/s00382-024-07396-8.

Funding This work was supported by the NASA Modeling, Analysis, and Prediction (MAP) program. Author LO also acknowledges support from the NASA MEASURES program.

Data availability The present work has not produced any original data. The datasets used in the analysis are all specified in the text and in the references.

Declarations

Ethical approval The authors have no conflicts of interest to disclose that are relevant to the content of this article.

References

Archer CL, Caldeira K (2008) Historical trends in the jet streams. Geophys Res Lett 35:l08803

Bender FA-M, Ramanathan V, Tselioudis G (2012) Changes in extratropical storm track cloudiness 1983–2008: Observational support for a poleward shift. Clim Dyn 38:2037–2053. https://doi.org/10.1007/s00382-011-1065-6

Bertrand L, Kay JE, Haynes J, De Boer G (2023) A Global gridded dataset for cloud vertical structure from combined cloudsat and CALIPSO observations preprint. ESSD – Global/meteorology. https://doi.org/10.5194/essd-2023-265

Byrne MP, Pendergrass AG, Rapp AD, Wodzicki K (2018) Response of the intertropical convergence zone to climate change: location, width, and strength. Curr Clim Change Rep 4:355–370. https://doi.org/10.1007/s40641-018-0110-5

Cesana GV, Del Genio AD (2021) Observational constraint on cloud feedbacks suggests moderate climate sensitivity. Nat Clim Chang 11(3):213–218. https://doi.org/10.1038/s41558-020-00970-y

Cho N, Tan J, Oreopoulos L (2021) Classifying planetary cloudiness with an updated set of MODIS cloud regimes. J App Meteorol Climatol. https://doi.org/10.1175/jamc-d-20-0247.1

Frey WR, Kay JE (2017) The influence of extratropical cloud phase and amount feedbacks on climate sensitivity. Clim Dyn 50:3097–3116

Grise KM, Coauthors, (2019) Recent tropical expansion: natural variability or forced response? J Climate 32:1551–1571. https://doi.org/10.1175/JCLI-D-18-0444.1

Grise KM, Davis SM, Staten PW, Adam O (2018) Regional and seasonal characteristics of the recent expansion of the tropics. J Climate 31:6839–6856. https://doi.org/10.1175/JCLI-D-18-0060.1

Hansen JE, Sato M, Simons L, Nazarenko LS, Sangha I, Kharecha P, Zachos JC, von Schuckmann K, Loeb NG, Osman MB, Jin Q, Tselioudis G, Jeong E, Lacis A, Ruedy R, Russell G, Cao J,

Li J (2023) Global warming in the pipeline. Oxford Open Clim. Change. 3(1):008. https://doi.org/10.1093/oxfclm/kgad008
Heidinger AK, Straka WC, Molling CC, Sullivan JT, Wu X (2010) Deriving an inter-sensor consistent calibration for the AVHRR solar reflectance data record. Int J Remote Sens 31:6493–6517
Heidinger AK, Foster MJ, Walther A, Zhao X (2013) The pathfinder atmospheres Extended (PATMOS-x) AVHRR Climate Data Set. Bull Amer Meteor Soc. https://doi.org/10.1175/BAMS-D-12-00246.1
Jakob C, Singh MS, Jungandreas L (2019) Radiative convective equilibrium and organized convection: An observational perspective. Journal of Geophysical Research: Atmospheres 124:5418–5430. https://doi.org/10.1029/2018JD030092
Karlsson K-G, Anttila K, Trentmann J, Stengel M, Fokke Meirink J, Devasthale A, Hanschmann T, Kothe S, Jääskeläinen E, Sedlar J, Benas N, van Zadelhoff G-J, Schlundt C, Stein D, Finkensieper S, Håkansson N, Hollmann R (2017) CLARA-A2 the second edition of the CM SAF cloud and radiation data record from 34 years of global AVHRR data. Atmos Chem Phys. https://doi.org/10.5194/acp-17-5809-2017
Karlsson KG et al (2023) CLARA-A the third edition of the AVHRR-based CM SAF climate data record on clouds, radiation and surface albedo covering the period submitted. Earth Syst Sci Data 15:4901–4926
Knapp KR, Young AH, Semunegus H, Inamdar AK, Hankins W (2021) Adjusting ISCCP Cloud Detection to Increase Consistency of Cloud Amount and Reduce Artifacts. J Atmos Ocean Technol 38:155–165. https://doi.org/10.1175/jtech-d-20-0045.1
Lau W, Kim K (2015) Robust Hadley circulation changes and increasing global dryness due to CO2 warming from CMIP5 model projections. Proc Natl Acad Sci USA 122:3630–3635
Loeb NG, Doelling DR, Wang H, Su W, Nguyen C, Corbett JG, Liang L, Mitrescu C, Rose FG, Kato S (2018) Clouds and the earth's radiant energy system (CERES) energy balanced and filled (EBAF) top-of-atmosphere (TOA) edition-4.0 data product. J Clim 31:895–918
Loeb NG, Johnson GC, Thorsen TJ et al (2021) Satellite and ocean data reveal marked increase in Earth's heating rate. Geophys Res Lett. https://doi.org/10.1029/2021GL093047
Mitchell JFB, Senior CA, Ingram WJ (1989) CO2 and climate: a missing feedback. Nature 341:132–134
Norris JR, Evan AT (2015) Empirical removal of artifacts from the ISCCP and PATMOS-x satellite cloud records. J Atmos Oceanic Technol 32:691–702. https://doi.org/10.1175/JTECH-D-14-00058.1
Norris JR, Allen RJ, Evan AT, Zelinka MD, O'Dell CW, Klein SA (2016) Evidence for climate change in the satellite cloud record. Nature 536:72–75. https://doi.org/10.1038/nature18273
Oreopoulos L, Cho N, Lee D, Kato S, Huffman GJ (2014) An examination of the nature of global MODIS cloud regimes. J Geophys Res 119:8362–8383. https://doi.org/10.1002/2013JD021409
Platnick S, Meyer K, Wind G, Holz RE, Amarasinghe N, Hubanks PA, Marchant B, Dutcher S, Veglio P (2021) The NASA MODIS-VIIRS continuity cloud optical properties products. Remote Sensing 13(1):2. https://doi.org/10.3390/rs13010002
Rind D, Rossow WB (1984) The effects of physical processes on the hadley circulation. J Atmos Sci 41:479–507. https://doi.org/10.1175/1520-0469(1984)041%3c0479:teoppo%3e2.0.co;2
Rossow WB, Ferrier J (2015) Evaluation of long-term calibrations of the AVHRR visible radiances. J Atmos Ocean Technol 32(4):744–766. https://doi.org/10.1175/JTECH-D-14-00134.1
Rossow WB, Knapp KR, Young AH (2022) International satellite cloud climatology project: extending the record. J Climate 35:141–158. https://doi.org/10.1175/JCLI-D-21-0157.1
Schiffer RA, Rossow WB (1983) The International satellite cloud climatology project (ISCCP): The first project of the world climate research programme. Bull Amer Meteorol Soc 64:779–784
Sherwood SC, Webb MJ, Annan JD, Armour KC, Forster PM, Hargreaves JC et al (2020) An assessment of Earth's climate sensitivity using multiple lines of evidence. Rev Geophys. https://doi.org/10.1029/2019rg000678
Staten PW, Coauthors, (2020) Tropical widening: from global variations to regional impacts. Bull Amer Meteor Soc 101:E897–E904. https://doi.org/10.1175/BAMS-D-19-0047.1
Stephens GL, Vane DG, Boain RJ, Mace GG, Sassen K, Wang Z, Illingworth AJ, O'Connor EJ, Rossow WB, Durden SL, Miller SD, Austin RT, Benedetti A, Mitrescu C, CloudSat Science Team (2002) The cloudsat mission and the a-train a new dimension of space-based observations of clouds and precipitation. Bull. Amer. Meteorol. Soc. 83:1771–1790. https://doi.org/10.1175/BAMS-83-12-1771
Stubenrauch CJ, Rossow WB, Kinne S, Ackerman S, Cesana G, Chepfer H, Di Girolamo L, Getzewich B, Guignard A, Heidinger A, Maddux BC, Menzel WP, Minnis P, Pearl C, Platnick S, Poulsen C, Riedi J, Sun-Mack S, Walther A, Winker D, Zeng S, Zhao G (2013) Assessment of global cloud datasets from satellites: project and database initiated by the GEWEX radiation panel. Bull Amer Meteorol Soc 94(7):1031–1049. https://doi.org/10.1175/BAMS-D-12-00117.1
Stubenrauch, C.J., S. Kinne, G. Mandorli, W.B. Rossow, D.M. Winker, S.A. Ackerman, H. Chepfer, L. Di Girolamo, A. Garnier, A. Heidinger, K.-G. Karlsson, K. Meyer, P. Minnis, S. Platnick, M. Stengel, S. Sun Mack, P. Vegho, A. Walther, X. Cai, A.H. Young and G. Zhao, 2024: Lessons learned from the updated GEWEX Cloud Assessment database. Surv. Geophys, (in press).
Tan J, Jakob C, Rossow WB, Tselioudis G (2015) Increases in tropical rainfall driven by changes in frequency of organized deep convection. Nature 519:451–454. https://doi.org/10.1038/nature14339
Tan I, Storelvmo T, Zelinka MD (2016) Observational constraints on mixed-phase clouds imply higher climate sensitivity. Science 352:224–227
Tselioudis G, Rossow W, Zhang Y, Konsta D (2013) Global weather states and their properties from passive and active satellite cloud retrievals. J Climate 26:7734–7746. https://doi.org/10.1175/JCLI-D-13-00024.1
Tselioudis G, Lipat B, Konsta D, Grise K, Polvani L (2016) Midlatitude cloud shifts, their primary link to the hadley cell, and their diverse radiative effects. Geophys Res Lett 43(9):4594–4601. https://doi.org/10.1002/2016GL068242
Tselioudis G, Rossow WB, Jakob C, Remillard J, Tropf D, Zhang Y (2021) Evaluation of clouds, radiation, and precipitation in CMIP6 models using global weather states derived from ISCCP-H cloud property data. J Climate 34:7311–7324. https://doi.org/10.1175/JCLI-D-21-0076.1
Webb MJ, Lock AP, Ogura T (2024) What are the main causes of positive subtropical low cloud feedbacks in climate models? J Adv Model Earth Syst. https://doi.org/10.1029/2023MS003716
Winker DM, Vaughan MA, Omar A, Hu Y, Powell KA (2009) Overview of the CALIPSO mission and CALIOP data processing algorithms. J Atmos Oceanic Technol 26:2310–2323. https://doi.org/10.1175/2009JTECHA1281.1
Wodzicki KR, Rapp AD (2016) Long-term characterization of the Pacific ITCZ using TRMM, GPCP, and ERA-Interim. J Geophys Res Atmos 121:3153–3170. https://doi.org/10.1002/2015JD024458
Woollings T, Drouard M, O'Reilly CH et al (2023) Trends in the atmospheric jet streams are emerging in observations and could be linked to tropical warming. Commun Earth Environ 4:125. https://doi.org/10.1038/s43247-023-00792-8

Xiong X, Butler JJ (2020) MODIS and VIIRS calibration history and future outlook. Remote Sens. https://doi.org/10.3390/rs-12-2523

Young AH, Knapp KR, Inamdar A, Hankins W, Rossow WB (2018) The international satellite cloud climatology project H-series climate data record product. Earth System Science Data 10(1):583–593. https://doi.org/10.5194/essd-10-583-2018

Zhang Y, Rossow WB (2023) Global radiative flux profile dataset: revised and extended. J Geophys Res Atmos. https://doi.org/10.1029/2022JD037340